Robotica (2009) volume 27, pp. 801–811. © Cambridge University Press 2008
doi:10.1017/S0263574708005146

Slip parameter estimation of a single wheel using a non-linear observer

Z. B. Song†, L. D. Seneviratne†, K. Althoefer†, X. J. Song†* and Y. H. Zweiri‡

†*Division of Engineering, King's College London, Strand, London WC2R 2LS, UK*
‡*School of Engineering, Mútah University, Karak, Jordon, 61710*

(Received in Final Form: September 5, 2008. First published online: October 9, 2008)

SUMMARY
Sliding mode observer is a variable structure system where the dynamics of a nonlinear system is altered via application of a high-frequency switching control. This paper presents a non-linear sliding mode observer for wheel linear slip and slip angle estimation of a single wheel based on its kinematic model and velocity measurements with added noise to simulate actual on-board sensor measurements. Lyapunov stability theory is used to establish the stability conditions for the observer. It is shown that the observer will converge in a finite time, provided the observer gains satisfy constraints based on a stability analysis. To validate the observer, linear and two-dimensional (2D) test rigs are specially designed. The sliding mode observer is tested under a variety of conditions and it is shown that the sliding mode observer can estimate wheel slip and slip angle to a high accuracy. It is also shown that the sliding mode observer can accurately predict wheel slip and slip angle in the presence of noise, by testing the performance of the sliding mode observer after adding white noise to the measurements. An extended Kalman filter is also developed for comparison purposes. The sliding mode observer is better in terms of prediction accuracy.

KEYWORDS: Sliding mode observer; Wheel slip and slip angle estimation; Autonomy; Single wheel; Extended Kalman filter.

1. Introduction

Wheeled vehicle linear slip and lateral slip angles are required for traction control and trajectory tracking purposes. However, the accurate measurement of wheel linear slip and slip angle is a complex problem.[1] Wheel linear slips are measured directly using a fifth wheel mounted to the rear bumper in ref. [2], but the uneven surface will lead to inaccuracy in encoder readings. A method for measuring vehicle slip angle using global positioning system (GPS) velocity measurements and gyro sensors is proposed in ref. [1]. However, GPS sometimes suffers from signal interferences and signal loss which results in inaccurate measurements of positions and velocities.[3]

* Corresponding author. E-mail: song.xiaojing@kcl.ac.uk

In ref. [4], linear slip is measured by comparing signals from wheel encoders and carriage encoders of a test bed and then used for identifying soil properties. However, measurements of encoders are subject to noise. A linear slip estimate method based on motor current measurements is proposed in ref. [5], while lateral slip angle is not considered. In ref. [6], a method to predict linear slip of a rover is presented using visual information of the terrain, which nevertheless requires prior knowledge of the terrain type.

Thus, indirect methods are used for the estimation of wheel linear slip and lateral slip angle based on readily available sensor measurements.

In ref. [7], an extended Kalman filter (EKF) is employed to estimate wheel slips and wheel slip angles based on a five-degree-of-freedom dynamic model of a wheeled vehicle and measurements including wheel angular velocity, acceleration and yaw rate. The use of an EKF to estimate wheel slip and slip angles of a tracked vehicle is examined in ref. [8]. However, track slip errors increase significantly during turning motions, since the EKF is essentially a linear observer for a non-linear system. An EKF is proposed to estimate slips of a wheeled loader in ref. [9]. It is shown that the slip experienced by the vehicle is significant particularly during cornering. An observer is developed in refs. [10, 11] to estimate the vehicle slip angle based on a dynamic model of a wheeled vehicle, with acceleration and yaw rate measurements.

In ref. [12], a sliding mode observer (SMO) is used to estimate the vehicle velocity from a wheel velocity based on the model for wheel dynamics, thus estimating slip while slip angle estimate is ignored. An SMO is proposed in ref. [13] to estimate vehicle slip angle only based on a simplified dynamic model of a wheeled vehicle. The slip angle estimate was compared with that measured by an optical sensor, and a second-order Markov-process is used to model lateral slip angle which is not applicable in practice. Further, this research does not study linear slip and traction dynamics. In ref. [14], longitudinal and lateral forces are estimated using an SMO. The error dynamics are proven to converge in a finite time interval while the nominal values of longitudinal and lateral forces limiting the applicability of the method. Also, the paper is not concerned with wheel slip and slip angle.

https://doi.org/10.1017/S0263574708005146 Published online by Cambridge University Press

In ref. [15], an Utkin SMO is proposed for wheel slip and slip angle estimation of a tracked vehicle. The robustness and superior performance of the SMO is demonstrated using experimental results.

An SMO is proposed to estimate wheel linear slip and slip angle in ref. [16], showing that the estimated wheel slip and slip angle have very good agreement with the measured ones and it is extended here with in-depth analysis of experimental results and detailed implementation of the SMO and the EKF.

Based on the work discussed in ref. [16], this paper demonstrates the robustness and high accuracy of the SMO using measured data from test rigs. The design of the SMO is based on a kinematic model and requires no prior knowledge of terrain properties and the observer proposed is capable of accurately estimating two slip parameters: wheel slip and slip angle of a single wheel, which characterises the steering behaviours.

Lyapunov theory is used to prove that the error dynamics converge after a finite time, provided the gains are selected to satisfy certain stability constraints. To the best of our knowledge, this is the first time that an SMO is used with a kinematic model to estimate wheel slip and slip angle of a single wheel. The SMO is validated by comparing the estimated wheel slip and slip angle, with those accurately measured using specially designed test rigs, showing very good agreement. Also an EKF is presented for comparison purposes.

The paper is structured as follows: In Section 2, the kinematic equations of the single wheel are presented. In Section 3, the SMO is developed and a rigorous stability analysis is given. Section 4 describes the experimental setup used to validate the proposed SMO. In Section 5, the SMO is validated by comparing estimates with the measured data, and conclusions are drawn in Section 6.

2. Single Wheel Kinematic Model with Slip Constraints

There are several papers on the kinematic modelling of wheeled vehicles.[17–20] In these studies, the contact between the wheel and the terrain is assumed to be a point of contact, and the kinematic equations are derived assuming pure rolling, considering no slip. The kinematic modelling of wheeled vehicles with slip constraints is seldom studied in the literature.

For a four-wheel car, each wheel has wheel slip and slip angle: linear slip and slip angle. One single wheel with steering characteristics exhibits these two behaviours, hence we investigate one-wheel car instead of a four-wheel car for the estimation of wheel slip angle (Fig. 1). In Fig. 1, $\alpha(\delta)$ represents either the slip angle or the steering angle as they are the same.[21]

The wheel can rotate about the y-axis and steer about z-axis, simulating a drive wheel of a car. There are two control inputs, steering angle δ and wheel angular velocity ω.

In Fig. 2, the linear slip of a wheel with respect to the terrain is defined as follows:

$$i = \frac{\omega r - V_x}{\omega r} = 1 - \frac{V_x}{\omega r} = -\frac{V_s}{\omega r}, \tag{1}$$

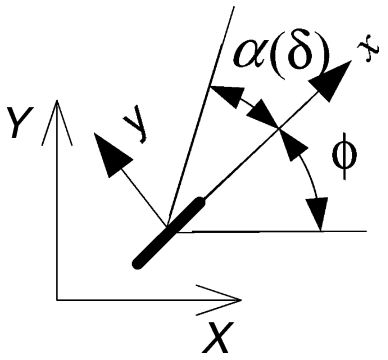


Fig. 1. Free body diagram of a single-wheel vehicle.

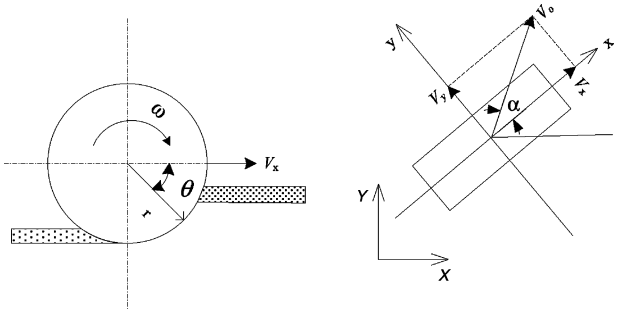


Fig. 2. Wheel velocities.

where, V_x, ω and V_s are the longitudinal, angular and slip velocities of the wheel, respectively, r is the radius of the wheel and (x, y) is a local frame attached to the wheel. The direction of wheel travel and the intersection line of the wheel plane with the road surface gives the slip angle, α (Fig. 2). From the velocity geometric relationship, the slip angle of the wheel is given by:

$$\alpha = \tan^{-1}\frac{V_y}{V_x}. \tag{2}$$

Given the vehicle velocity V_0 and slip angle α (Fig. 2) , $\dot{X}$ and $\dot{Y}$ can be computed as

$$\dot{X} = \cos(\alpha + \phi)\frac{V_x}{\cos\alpha}, \tag{3}$$

$$\dot{Y} = \sin(\alpha + \phi)\frac{V_x}{\cos\alpha}. \tag{4}$$

Using velocity relationships, kinematic equations (1), (3) and (4) can be simplified to give the following equations:

$$\dot{X} = V_x[\cos\phi - \tan\alpha\sin\phi], \tag{5}$$

$$\dot{Y} = V_x[\sin\phi + \tan\alpha\cos\phi], \tag{6}$$

$$\dot{\theta} = \omega = \frac{V_x}{r(1-i)}, \tag{7}$$

where, θ is the angular displacement of the single wheel.

Thus, given the vehicle forward velocity V_x, the vehicle heading direction ϕ, wheel slip and slip angle (i, α), the wheel angular velocity ω and wheel radius r, the vehicle velocity in global coordinates $(\dot{X}, \dot{Y}, \dot{\theta})$ can be estimated

https://doi.org/10.1017/S0263574708005146 Published online by Cambridge University Press

from Eqs. (5)–(7). Also given $(\dot{X},\ \dot{Y},\ \dot{\theta})$, V_x, ϕ and r, the above equations can be inverted to find wheel slip and slip angle, $(i,\ \alpha)$.

$$i = 1 - \frac{V_x}{\dot{\theta} r}, \tag{8}$$

$$\alpha = \sqrt{\frac{V_x^2}{\dot{X}^2 + \dot{Y}^2}}. \tag{9}$$

3. Sliding Mode Observer

In a general system, not all state variables may be measured using sensors. An observer allows the estimation of those unmeasurable state variables based on readily available measurements. A Kalman filter is used to estimate wheel slip and slip angle of a vehicle in ref. [8]. The kinematic model is linearised at a nominal trajectory and states updated where the mean-square error is minimised. In general, sensor measurements are prone to noise, and the observers have to be robust against noise and other external disturbances.

SMOs are increasingly used in many different applications[13–16] and are popular approaches to reconstruct states in non-linear systems since they can deal with noise and uncertainty in non-linear dynamic systems.[22, 23] This paper presents a non-linear SMO for the estimation of wheel slip and slip angle of a single wheel based on its kinematic model and feedback from simple sensors like global positioning systems. The SMO minimizes the errors between the predicted and measured vehicle trajectories, converging the estimated states to the real states, and thereby estimating wheel slip and slip angle. With an SMO, the control action switches between values in a finite time, and this may cause chattering; a low pass filter is used to smooth the discontinuous terms. The SMO designed in this study constructs a supplementary system with a discontinuous switching component, and then intentionally creates a sliding motion in the supplementary system.[24]

3.1. Design of the sliding mode observer

The methodology used here is based on the sliding mode design principles presented in refs. [22, 23]. This basic principle is extended here to estimate wheel slip and slip angle (i, α) using Eqs. (5) and (7), which is a multi-input and multi-output system.

In this study, the state variables to be estimated are wheel slip and slip angle i and α. In the previous research, up to two state variables are estimated using an SMO.[24] An SMO is presented to estimate the indicated engine torque and the load torque of a diesel engine from crankshaft and coupling angular velocity measurements, where the two state variables are uncoupled. However, the kinematics of a single wheel are coupled. Hence, the vehicle linear velocity V_x is assumed to be known and used to decouple wheel slip and wheel slip angle from the kinematic model and design an SMO.

It is noted that Eq. (5) or (6) can be used to estimate the slip angle and Eq. (7) is used to estimate wheel slip i.

The SMO for a single wheel is designed as follows:

$$\dot{\hat{X}} = V_x \cos\phi + L_1 \text{sign}(X - \hat{X}) + L_2(X - \hat{X}), \tag{10}$$

$$\dot{\hat{\theta}} = L_3 \text{sign}(\theta - \hat{\theta}) + L_2(\theta - \hat{\theta}), \tag{11}$$

where, $\hat{X}$ and $\hat{\theta}$ are estimates of X and θ, respectively. L_1, L_2 and L_3 are sliding gains, L_2 is a positive number.

Subtracting Eq. (5) from Eq. (10) and Eq. (7) from Eq. (11) yields the error dynamics:

$$\dot{\bar{X}} = -V_x \sin\phi \tan\alpha - L_1 \text{sign}(X - \hat{X}) - L_2(X - \hat{X}), \tag{12}$$

$$\dot{\bar{\theta}} = \frac{V_x}{r(1-i)} - L_3 \text{sign}(\theta - \hat{\theta}) - L_2(\theta - \hat{\theta}). \tag{13}$$

When the error dynamics reach the sliding mode, i.e. $\bar{X} \approx 0$ and $\bar{\theta} \approx 0$, i.e. $X \to \hat{X}$ and $\phi \to \hat{\phi}$, Eqs. (12) and (13) become

$$-V_x \sin\phi \tan\alpha - L_1 \text{sign}(X - \hat{X}) - L_2(X - \hat{X}) \approx 0, \tag{14}$$

$$\frac{V_x}{r(1-i)} - L_3 \text{sign}(\theta - \hat{\theta}) - L_2(\theta - \hat{\theta}) \approx 0. \tag{15}$$

Given the longitudinal velocity of a wheel, V_x, sliding gains, L_1, L_2, L_3 and trajectory X, θ, wheel slip and slip angle can then be calculated from Eqs. (14) and (15).

$$\alpha = \pm \cos^{-1} \sqrt{\frac{V_x^2 \sin^2\phi}{(L_1 \text{sign}(X - \hat{X}))_{\text{eq}}^2 + V_x^2 \sin^2\phi}} \tag{16}$$

$$i = 1 - \frac{V_x}{(L_3 \text{sign}(\theta - \hat{\theta}))_{\text{eq}} r}, \tag{17}$$

where $(\cdot)_{\text{eq}}$ represents a lowpass filter[22] used to smooth estimated wheel slip and slip angle derived from the discontinuous SMO outputs. Then, given the sprocket wheel speed ω, sliding gains L_1, L_2, L_3, V_x and the vehicle and wheel trajectories X, θ, wheel slip and slip angle can be found. The terms $(L_1 \text{sign}(X - \hat{X}))_{\text{eq}}$ and $(L_3 \text{sign}(\theta - \hat{\theta}))_{\text{eq}}$ are determined using a first-order linear filter with filter output z and filter time constant μ:

$$\mu \dot{z} + z = L \text{sign}(x) \tag{18}$$

indicating that $\lim_{\mu \to 0} z = x$, where x represents the discontinuous terms $(L_1 \text{sign}(X - \hat{X}))_{\text{eq}}$ and $(L_3 \text{sign}(\theta - \hat{\theta}))_{\text{eq}}$, L is the sliding gain and μ is the filter time constant (a value between 0 and 1).[22]

An alternative algorithm for wheel slip and slip angle using an EKF is presented in Appendix A.

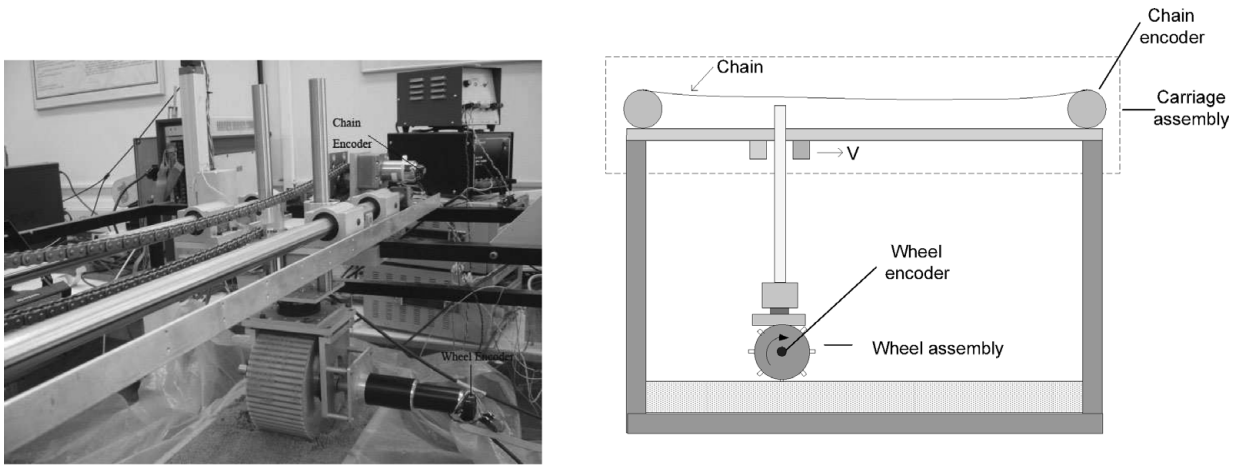
3.2. Stability analysis and selection of sliding gains

After the design of the structure of the SMO, a Lyapunov stability analysis is conducted to find convergence criteria of the system and hence choose the sliding gains.

Let the switching functions be

$$s_1 = X - \hat{X}, \quad s_2 = \theta - \hat{\theta}. \tag{19}$$

https://doi.org/10.1017/S0263574708005146 Published online by Cambridge University Press



(a) Single-wheel test rig

(b) Schematic of the single-wheel test rig

Fig. 3. Linear test rig.

For stability, the SMO dynamics must exhibit the following characteristics: The error state must reach the sliding surface from an arbitrary point in error space in a finite time and the error dynamics must be stable in some neighbourhood of the sliding surface.

Let Lyapunov functions be $V_n = \frac{1}{2}s_n^2$, where $n = 1, 2, \ldots$. For, $n = 1$, from Eq. (12)

$$\dot{V}_1 = s_1\dot{s}_1 = -V_x \sin\phi \tan(\alpha)s_1 - L_1\text{sign}(s_1)s_1 - L_2 s_1^2 \leq |V_x \sin\phi \tan\alpha|\,|s_1| - L_1\,|s_1| < 0. \quad (20)$$

Hence, if

$$L_1 > |V_x \sin\phi \tan\alpha|$$

then $\dot{V}_1 < 0$.

Similarly, for $n = 2$, from Eq. (13)

$$\dot{V}_2 = s_2\dot{s}_2 = \frac{V_x}{r(1-i)}s_2 - L_3\text{sign}(s_2)s_2 - L_2 s_2^2 \leq \left|\frac{V_x}{r(1-i)}\right| |s_2| - L_3\,|s_2|\,. \quad (21)$$

Hence, if

$$L_3 > \left|\frac{V_x}{r(1-i)}\right|^+$$

then $\dot{V}_2 < 0$.

If, the sliding gains satisfy the following conditions:

$$L_1 \geq |V_x|^+\,|\tan\alpha|^+ \quad (22)$$

$$L_2 > 0 \quad (23)$$

$$L_3 \geq \left|\frac{V_x}{r(1-i)}\right|, \quad (24)$$

where $|\cdot|^+$ represents upper bound; following up from the above stability analysis, the sliding gains are selected: L_1 is $|V_x|^+$ if α is less than 45° while L_1 can be tuned if α can be expected to be larger; L_2 is a small positive number; L_3 is $|\frac{V_x}{2r}|^+$.

4. Experimental Setup

The algorithm is tested on specially designed linear and 2D test rigs where wheel slip and slip angle can be accurately measured and controlled. Each test is repeated three times and average readings are taken.

4.1. Linear test rig

Figures 3(a) and 3(b) show a linear test rig with a single wheel used for algorithm validation. The linear test rig consists of a wheel assembly and a carriage assembly. The wheel assembly is not vertically constrained and can move up and down freely.

During experiments, two motors, one driving the wheel and another driving the chain attached to the carriage, are operated at different speeds to generate various wheel slip values. The experimental soils are contained in a soil box $0.1 \times 0.85 \times 0.8$ m^3. The SMO and the EKF require the carriage velocity V_x and wheel angular displacement θ, respectively, as inputs. V_x and θ are measured by a chain motor encoder and a wheel motor encoder, respectively (Fig. 3). The resolutions of the chain and the wheel encoders are 23,000 pulses per revolution, which with a motor gear ratio of 500:1 and a sampling rate 1 Hz, gives a linear velocity resolution of 6×10^{-4} m/s.

The following gives a summary of the linear rig parameters:

Carriage

Weight:	7.43 kg
Size:	0.4 m × 0.3 m × 0.01 m
Speed:	range: 0–0.05 m/s and accuracy: 6×10^{-4} m/s
Position:	range: 0–0.9 m and accuracy: 6×10^{-4} m

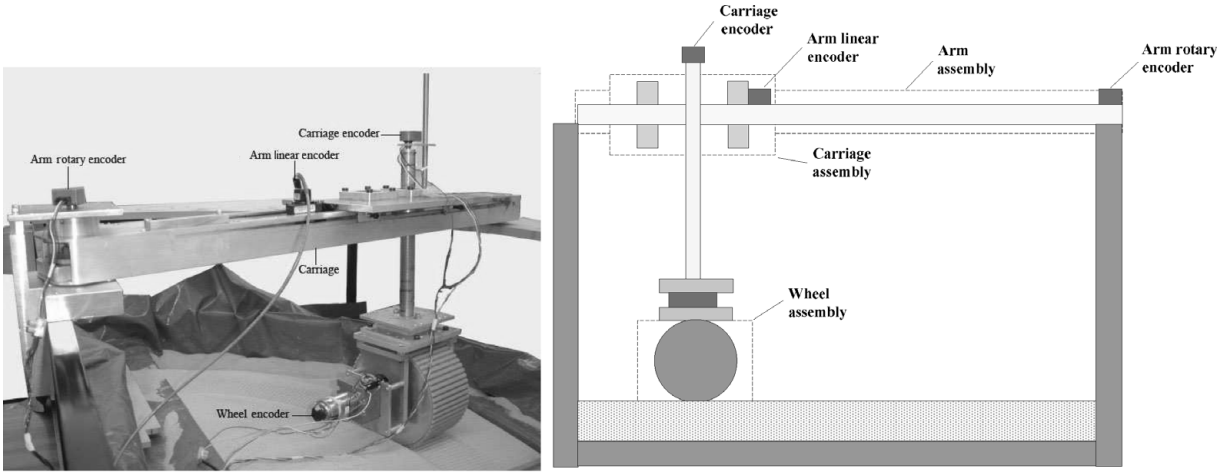
Wheel

Weight:	4.650 kg/7.850 kg
Size/wheel:	diameter: 0.198 m and width: 0.098 m
Speed:	range: 0–0.05 m/s and accuracy: 6×10^{-4} m/s
Position:	range: 0–0.9 m and accuracy: 6×10^{-4} m

Slip

Slip:	range: 0–90%

https://doi.org/10.1017/S0263574708005146 Published online by Cambridge University Press



(a) 2D test rig (b) Schematic of a 2D test rig

Fig. 4. 2D test rig.

4.2. 2D test rig

The linear test rig simulates one degree of freedom, X motion of the carriage assembly. This is extended to three degrees of freedom (X, Y and θ), motion in the 2D test rig, by attaching the carriage to an arm, as shown in Fig. 4(a). The 2D test rig can simulate arbitrary wheel movements in X, Y and θ directions.

The arm can rotate about arm rotational centre and the carriage can rotate about its axis, and translate along the arm, to provide the three degrees of freedom. The 2D test rig has two actuators; one for the carriage, the other actuator for the wheel assembly.

The 2D test rig consists of a wheel assembly, a carriage assembly and an arm assembly [Figs. 4(a) and 4(b)]. It is noted that the carriage imposes no restriction on vertical motion of the wheel assembly and hence the wheel assembly can move up and down freely. The arm can rotate about a vertical axis, θ_1 and the carriage can move along the arm, r_1 and rotate about a vertical axis.

The experimental soils are contained in a cylindrical container with a diameter of 0.85 m and height of 0.15 m.

The SMO and the EKF require measurements of V_x, X, ϕ and θ as inputs. Four sensors, an arm rotary encoder θ_1, arm linear encoder θ_2, a wheel motor built-in encoder ω and a linear position transducer r are used to measure V_x, X, ϕ and θ. ϕ is measured by the arm rotational and carriage encoders (Fig. 5).

$$\phi = \theta_1 + \theta_2.$$

X is measured by arm rotary and linear encoders [Figs. 4(a) and 4(b)]:

$$X = r\cos\theta_1.$$

V_x is measured by the arm linear encoder, the arm rotary encoder and the carriage encoder.

$$V_x = \sqrt{(\dot{r}\cos\theta_1 - r\sin\theta_1\dot{\theta}_1)^2 + (\dot{r}\sin\theta_1 + r\cos\theta_1\dot{\theta}_1)^2}\cos\alpha,$$

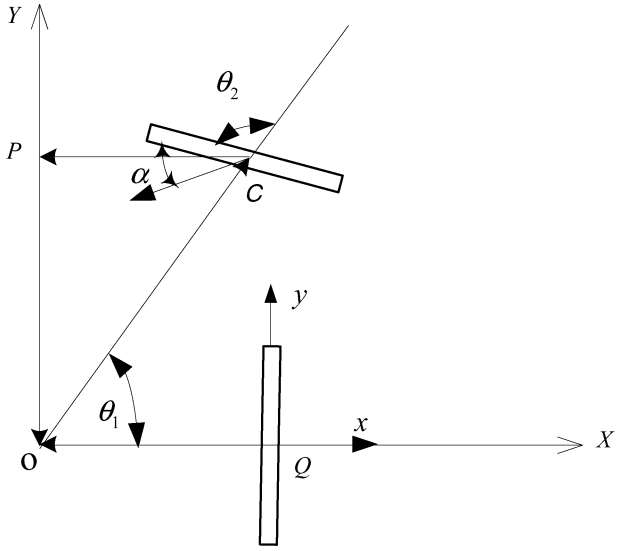


Fig. 5. Loop velocity vector diagram.

where α is the angle between the velocity of vehicle and wheel plane.

$$\alpha = \tan^{-1}\frac{\dot{r}\sin\theta_1 + r\cos\theta_1\dot{\theta}_1}{\dot{r}\cos\theta_1 - r\sin\theta_1\dot{\theta}_1},$$

where θ_1 and $\dot{\theta}_1$ are measured using the arm rotary encoder, θ_2 and $\dot{\theta}_2$ are measured using the carriage encoder (see Fig. 5).

The slip and slip angle measurement approach is described in detail in Appendix B.

Then the 2D test rig parameters are given as follows:

Carriage

Weight: 3.680 kg
Size: 0.4 m × 0.3 m × 0.01 m
Speed: range: 0–0.2 m/s and accuracy: 0.207×10^{-3} m/s
Position: range: 0–0.9 m and accuracy: 0.207×10^{-3} m

Wheel

Weight: 7.850 kg
Size/wheel: diameter: 0.198 m and width: 0.098 m

https://doi.org/10.1017/S0263574708005146 Published online by Cambridge University Press

Table I. Soil parameters (c: cohesion; φ: friction angle; K: shear deformation modulus).

Soil types	c (kPa)	φ (rad)	K (m)
Garside 14/25 sand	0	34	0.002
Garside 60 sand	0	30	0.001
Garside Iron sand	3	33	0.0011

Speed: range: 0–0.05 m/s and accuracy: 6×10^{-4} m/s
Position: range: 0–0.9 m and accuracy: 6×10^{-4} m

Slip

Slip: range: 0–90%

While, the SMO for a wheeled vehicle receives X, V_x, θ as inputs and then estimates wheel slip and slip angle after converging the estimated states to real states.

5. Experimental Results

Test rigs measure all the parameters, hence the sliding mode algorithm can be tested for linear and 2D motions.

The wheel assembly is driven to travel on three types of soils, whose properties are given in Table I. The soils, provided by Aggregate Industries, UK, are classified as dried sand (Garside 14/25 sand and Garside 60 sand) and damp Garside Iron sand. The depth of soils during experiments is 80 mm.

5.1. Linear test rig

The difference in velocities of the two drive motors will generate variable slip ratios, and the wheel slip can be accurately measured and controlled in this manner.

In test I, Garside 14/25 sand is used. Figure 6 shows the comparison between the measured and estimated slips using the SMO and the EKF. The SMO estimates converge to the measured ones after 5 s. The sliding gains L_2 and L_3 are 0.06 s^{-1} and 1.60 s^{-1}, respectively, where gains are chosen according to the stability analysis.

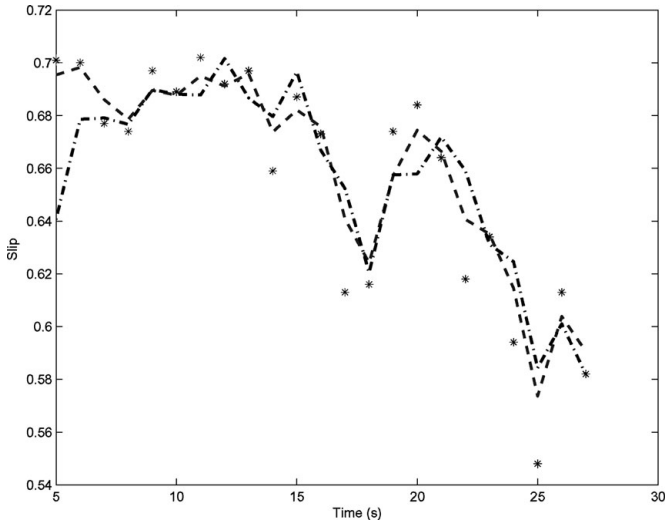


Fig. 6. Test I: The measured slip (***) and the estimated slip using the SMO (- - -) and the EKF (- · - · -) (Garside 14/25 sand).

Table II. Test I: Garside 14/25 sand for wheel with linear test rig.

Slip ranges (%)	Mean RMS error using SMO (%)	Mean RMS error using EKF (%)
0–10	10.42	19.56
10–20	10.28	32.66
20–30	8.57	15.76
30–40	9.98	34.77
40–50	3.13	6.64
50–60	1.73	3.04
60–70	2.29	5.46
70–90	1.39	5.02

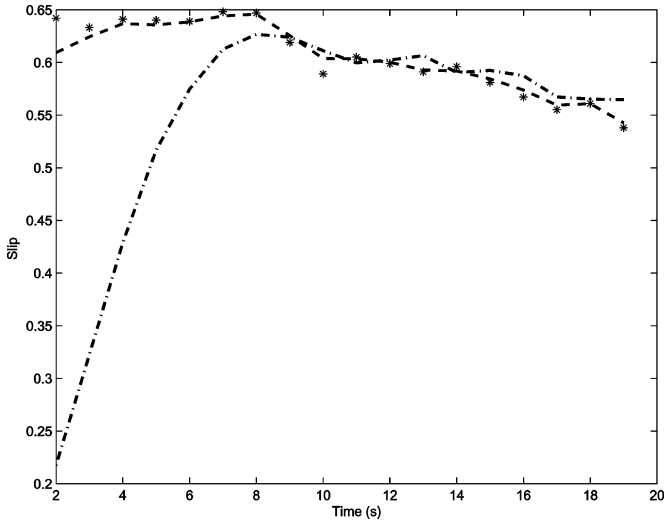


Fig. 7. Test II: The measured slip (***) and the estimated slip using the SMO (- - -) and the EKF (- · - · -) (Garside 60 sand) for wheel with linear test rig.

Table II shows the RMS errors for slip estimates over a range of slip values, from 0–90% using the SMO and the EKF.

In test II, Garside 60 sand is used. Figure 7 shows the comparison between the measured and estimated slips using the SMO and the EKF. The slip estimates using the SMO converge to the measured ones after 2 s.

The sliding gains L_2 and L_3 are 0.06 s^{-1} and 8 s^{-1}, respectively.

Table III shows the RMS errors for slip estimates over a range of slip values, from 0–90% using the SMO and the EKF.

Table III. Test II: Garside 60 sand for wheel with linear test rig.

Slip ranges (%)	Mean RMS error using SMO (%)	Mean RMS error using EKF (%)
0–10	15.52	40.61
10–20	6.45	11.85
20–30	7.47	11.04
30–40	4.53	6.68
40–50	2.62	9.32
50–60	1.9	5.76
60–70	5.34	17.31
70–90	1.39	5.02

https://doi.org/10.1017/S0263574708005146 Published online by Cambridge University Press

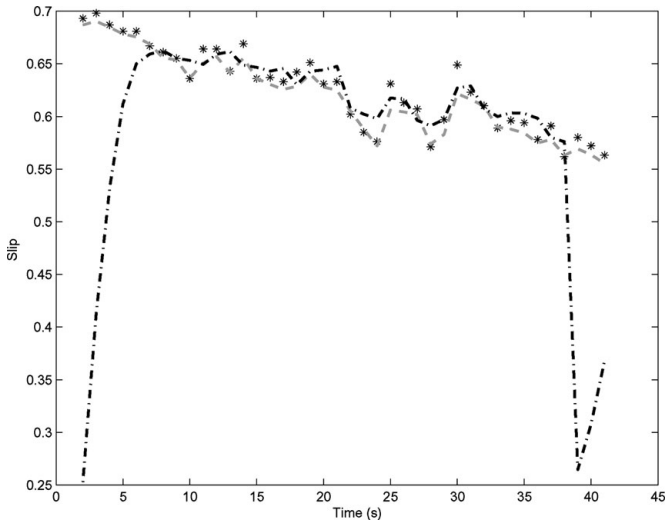


Fig. 8. Test III: The measured slip (***) and the estimated slip using the SMO (- - -) and the EKF (- · - · -) (Garside Iron sand) for wheel with linear test rig.

Table IV. Test III: Garside Iron sand for wheel with linear test rig.

Slip ranges (%)	Mean RMS error using SMO (%)	Mean RMS error using EKF (%)
0–10	14.36	25.38
10–20	7.96	13.66
20–30	2.59	6.68
30–40	7.06	13.99
40–50	8.23	31.71
50–70	1.99	5.46
70–90	2.81	6.1

In test III, Garside Iron sand is used. Figure 8 shows the comparison between the measured and the estimated slips using the SMO and the EKF. The estimates converge to the measured ones after 2 s. The sliding gains L_2 and L_3 are 0.06 s^{-1} and 2 s^{-1}, respectively. After 38 s, the EKF starts to diverge significantly. For this test, significant vibrations are observed at the finish time and this may cause the estimate of the EKF to deviate largely from the real values.

Table IV shows the RMS errors for slip estimates over a range of slip values, from 0–70% using the SMO and the EKF.

Table V shows the mean RMS errors in slip estimate for tests I, II and III under two scenarios: measurement data as inputs and measurement data with white noise as inputs. White noise, of magnitude up to ±5% the measurements, is added to the measurement signals to test the robustness of the

Table V. The mean RMS error in i is measured in these two scenarios.

	Without noise		With noise	
Test sets	SMO (%)	EKF (%)	SMO (%)	EKF (%)
Test I	1.73	3.04	2.99	3.90
Test II	2.62	9.32	5.8	15.7
Test III	1.99	5.46	2.97	10.53

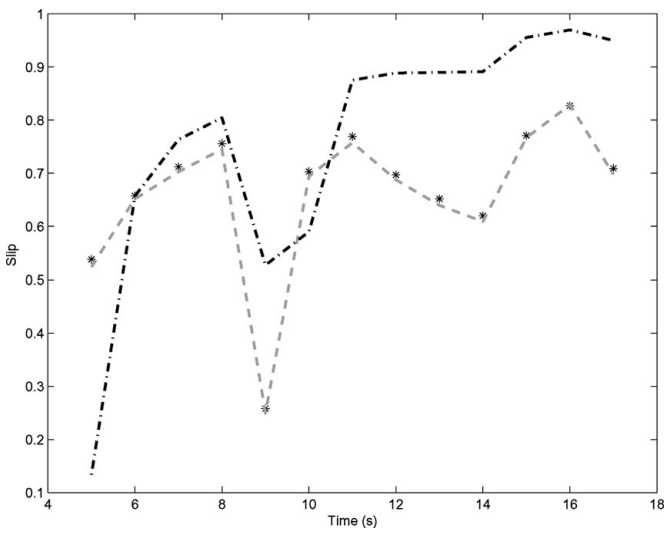


Fig. 9. Test I: The measured slip (***) and the estimated slip using the SMO (- - -) and the EKF (- · - · -) (Garside 14/25 sand) for wheel with 2D test rig.

SMO and the EKF. It is seen that the SMO is robust against noise.

5.2. 2D test rig results

A single-wheel assembly is commanded to run on the 2D test rig in Fig. 4(a). The SMO is tested on a variety of slip ranges, soils and speeds.

In test I, Garside 14/25 sand is used. Figures 9 and 10 show the measured and the estimated wheel slips and slip angles using the SMO and the EKF, respectively.

Table VI shows the estimated wheel slips and slip angles using the SMO and the EKF for a range of slip values, from 0% to 90%.

In test II, Garside 60 sand is used. Figures 11 and 12 show the measured and the estimated wheel slips and slip angles using the SMO and the EKF. The sliding gains L_1, L_2 and L_3 are selected as 0.03 s^{-1}, 0.06 s^{-1} and 0.46 s^{-1}. It is noted that

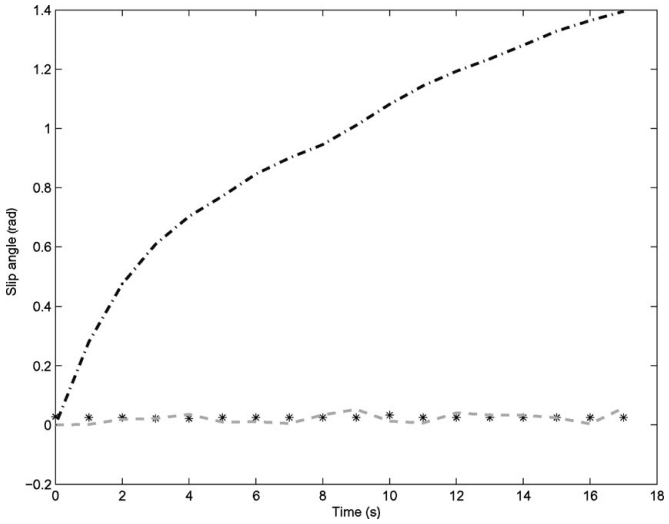


Fig. 10. Test I: The measured slip angle (***) and the estimated slip angle using the SMO (- - -) and the EKF (- · - · -) (Garside 14/25 sand) for wheel with 2D test rig.

https://doi.org/10.1017/S0263574708005146 Published online by Cambridge University Press

Table VI. Test I: Garside sand 14/25 for wheel with 2D test rig.

	Mean RMS error in i		Mean RMS error in α	
Slip ranges (%)	SMO (%)	EKF (%)	SMO (%)	EKF (%)
0–10	18.47	20.73	10.37	41.44
10–20	8.04	45.62	23.76	44.89
20–30	3.80	21.62	8.44	39.40
40–50	3.39	19.72	6.70	34.88
50–70	1.30	6.50	3.78	15.11
70–90	3.04	13.36	4.07	26.47

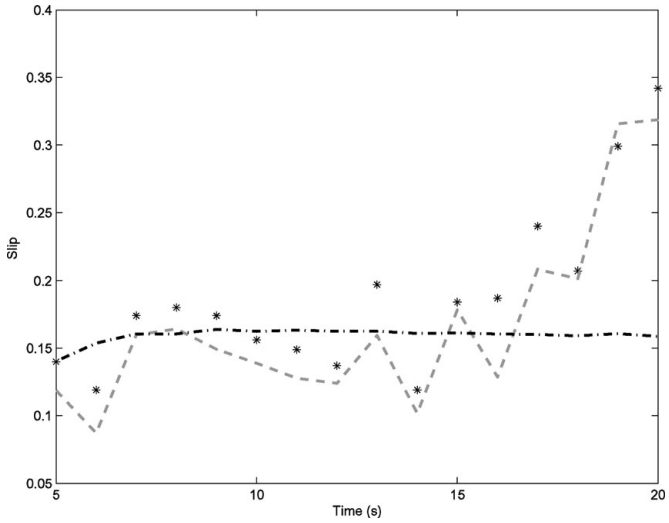


Fig. 11. Test II: The measured slip (***) and the estimated slip using the SMO (- - -) and the EKF (- · - · -) (Garside 60 sand) for wheel with 2D test rig.

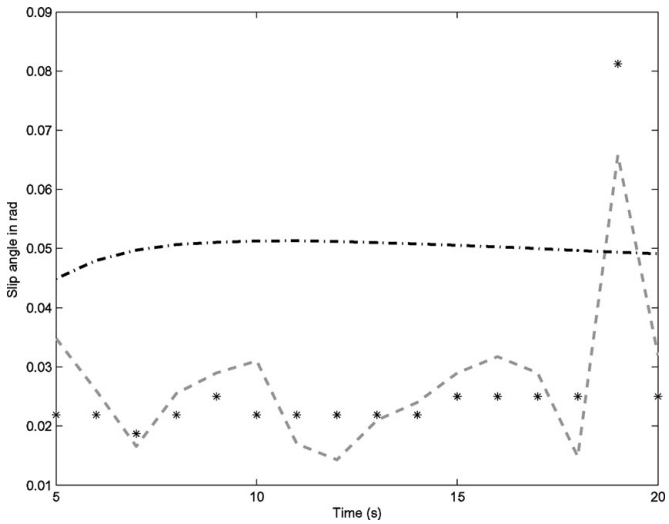


Fig. 12. Test II: The measured slip angle (***) and the estimated slip angle using the SMO (- - -) and the EKF (- · - · -) (Garside 60 sand) for wheel with 2D test rig.

slip angle prediction in particular has large oscillations while the input is relatively constant as the 2D test rig is turning abruptly in the last seconds when a large steering torque is applied to the wheel.

Table VII. Test II: Garside sand 60 for wheel with 2D test rig.

	Mean RMS error in i		Mean RMS error in α	
Slip ranges (%)	SMO (%)	EKF (%)	SMO (%)	EKF (%)
0–10	14.85	20.82	7.82	16.45
10–20	14.12	20.23	12.85	128.36
20–30	13.47	20.98	10.17	18.54
40–50	2.75	16.50	5.56	29.45
50–70	1.48	7.90	3.32	17.54

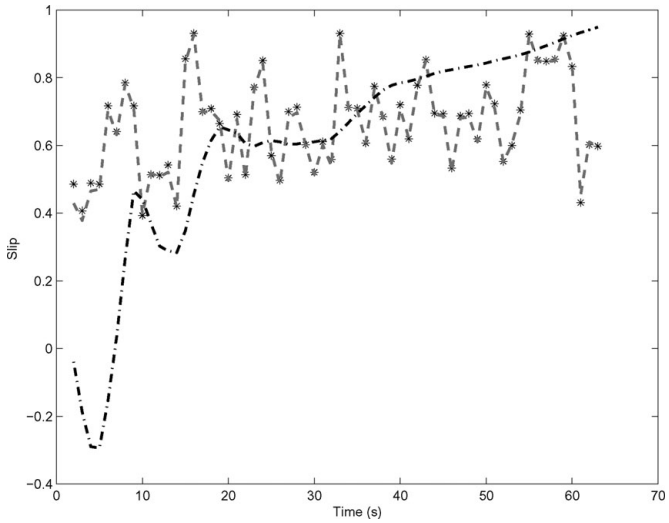


Fig. 13. Test III: The measured slip (***) and the estimated slip using the SMO (- - -) and the EKF (- · - · -) (Garside Iron sand) for wheel with 2D test rig.

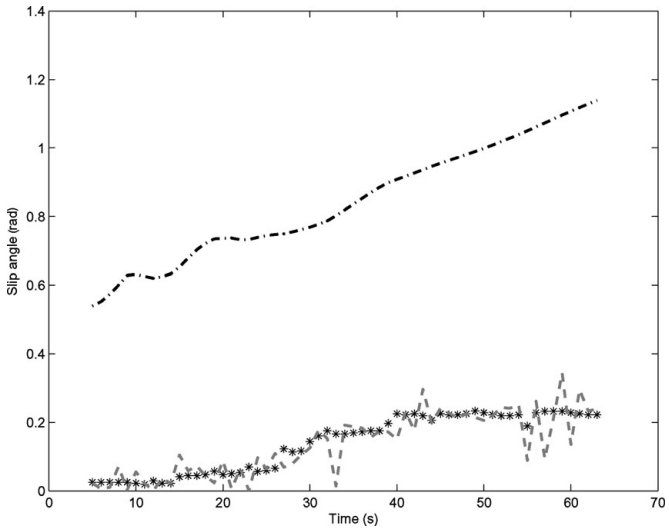


Fig. 14. Test III: The measured slip angle (***) and the estimated slip angle using the SMO (- - -) and the EKF (- · - · -) (Garside Iron sand) for wheel with 2D test rig.

Table VII shows the estimated wheel slips and slip angles using the SMO and the EKF for a range of slip values, from 0% to 50%.

In test III, Garside Iron sand is used. Figures 13 and 14 show the measured and the estimated wheel slips and slip

https://doi.org/10.1017/S0263574708005146 Published online by Cambridge University Press

Table VIII. Test III Garside Iron sand for wheel with 2D test rig.

	Mean RMS error in i		Mean RMS error in α	
Slip ranges (%)	SMO (%)	EKF (%)	SMO (%)	EKF (%)
0–10	3.58	12.11	6.22	21.52
10–20	11.09	61.91	8.63	88.21
20–30	2.40	15.69	5.74	29.31
40–50	2.07	12.90	4.46	20.22
50–70	1.48	10.84	5.17	12.86

angles using the SMO and the EKF, respectively. The sliding gains L_1, L_2 and L_3 are selected as 0.15 s^{-1}, 0.06 s^{-1} and 2.33 s^{-1}.

Table VIII shows the estimated wheel slip and slip angle using the SMO and the EKF, for a range of slip values, from 0% to 50%.

The mean RMS errors in wheel slip and slip angle estimates for tests I, II and III are summarised in Table IX. In this table, symbols A and B represent mean RMS errors in wheel slip with measurement data and measurement data with added noise, respectively, while symbols C and D represent mean RMS errors in wheel slip angle with measurement data and measurement data with added noise, respectively.

To test the robustness of the SMO and the EKF, white noise, with a magnitude of up to ±5% of measured signals, is superimposed on the measured signals. In Table IX, it is seen that the SMO is robust against noise.

5.3. Summary

In summary, a single-wheel assembly is tested on three types of sands, Garside 14/25 sand, Garside 60 sand and Garside Iron sand using the linear and 2D test rigs. The proposed SMO is tested on a variety of slip ranges, from 0% to 99% and speeds, from 0 m/s to 0.05 m/s.

Tables II–IV show that the SMO is better than the EKF in terms of prediction accuracy. Table V shows that the SMO is robust against noise.

Linear case is then extended to a 2D case where rotation is included. Tables VI–VIII also show that the SMO is better in terms of prediction accuracy.

In Figs. 10, 12 and 14, the slip angle estimate is about one radian from the actual measured values for the EKF. There are two main reasons to explain why the slip angle estimate for the EKF is so far off: one is due to modelling errors, where wheel slip and slip angle are assumed to be slowly time-varying while in practice wheel slip angle experiences abrupt changes especially when the vehicle is steering; another one is that an EKF is a linear observer for a highly non-linear kinematic model of a vehicle and need to linearise kinematic equations, i.e., a linear observer is applied to a non-linear case.

The assumption mentioned above is a general assumption with Kalman filter designed by other researchers[7,25] and evidenced by experimental results.

It is observed that vibrations are significant when wheel slip and slip angle are relatively low. The noise caused by vibrations affects the accuracy of slip estimate.

6. Conclusions and Future Work

This paper presents a non-linear SMO to estimate wheel linear slip and slip angle of a single wheel. Lyapunov theory is used to prove the convergence of error dynamics of the SMO. The sliding gains are chosen according to stability criteria. To validate the observer proposed, linear and 2D test rigs are specially designed to accurately measure wheel slip and the slip angle. A single wheel was commanded to move on three types of soils at various slip values from 0% to 90%. The measured and the estimated wheel slip and slip angle from the SMO and the EKF are compared to validate the algorithms. Experimental results show that the estimated wheel slip and slip angle using the SMO have very good agreement with measured ones, (error range 0–15%) as shown in Tables II–IV. However, the estimated wheel slip and slip angle using the EKF are less accurate (error range 14–141%). The SMO is shown to be robust against the noise.

In order to implement the SMO algorithm in unmanned ground vehicles, sensors to measure the vehicle longitudinal velocity and vehicle trajectory are required. Of currently available sensing system, sensors such as GPS, DGPS, inertial sensors (particularly for high acceleration), visual odometry-based sensors or a combination of above sensors, could provide the necessary observer inputs to implement the proposed algorithm.[26,27] Work at King's College London is underway to test the SMO algorithm based on an integrated visual odometry and inertial sensors.[28]

Table IX. Mean RMS errors.

	A		B		C		D	
Test sets	SMO (%)	EKF (%)	SMO (%)	EKF (%)	SMO (%)	EKF (%)	SMO (%)	EKF (%)
Test I	3.04	3.36	10.04	39.49	6.78	17.36	10.04	39.49
Test II	14.85	20.82	17.98	25.5	7.82	16.45	10.09	19.64
Test III	1.69	8.15	5.95	20.7	3.84	14.93	12.39	18.42

https://doi.org/10.1017/S0263574708005146 Published online by Cambridge University Press

References

1. D. M. Bevly, J. C. Gerdes, C. Wilson and G. Zhang, "The Use of GPS Based Velocity Measurements for Improved Vehicle State Estimation," *Proceeding of the American Control Conference,* Chicago, IL (2000) pp. 2538–2542.
2. C. Lee, K. Hedrick and K. Yi, "Real-time slip-based estimation of maximum tire-road friction coefficient," *IEEE/ASME Trans. Mechatron.* **9**(2), 454–458 (Jun. 2004).
3. X. J. Song, L. Seneviratne, K. Althoefer and Z. B. Song, "Vision-based velocity estimation for unmanned ground vehicles," *Int. J. Info. Acquis.* **4**(4), 303–325 (2007).
4. K. Iagnemma and S. Dubowsky, *Mobile Robots in Rough Terrain: Estimation, Motion Planning and Control with Application to Planetary Rovers*, vol. 12 (Springer-Verlag, Berlin, Heidenlberg, 2004).
5. L. Ojeda, D. Cruz, G. Reina and J. Borenstein, "Current-based slippage detection and odometry correction for mobile robots and planetary rovers," *IEEE Trans. Rob.* **22**, 366–378 (2006).
6. A. Angelova, L. Matthies, D. Helmick, G. Sibley and P. Perona, "Learning to Predict Slip for Ground Robots," *Proceedings of the IEEE International Conference on Robotics and Automation,* Orlando, FL (2006) pp. 3324–3331.
7. L. Ray, "Nonlinear tire force estimation and road friction identification: Simulation and experiments," *Automatica* **33**(10), 1819–1833 (1997).
8. A. T. Le, "Estimation of Track-soil Interactions for Autonomous Tracked Vehicles," *Proceedings of the IEEE International Conference on Robotics and Automation,* Albuquerque, New Mexico, New York, vol. 2 (1997) pp. 1388–1393.
9. S. Scheding, G. Dissanayake, E. M. Nebot and H. Durrant-Whyte, "An experiment in autonomous navigation of an underground mining vehicle," *IEEE Trans. Rob. Automat.* **15**(1), 85–95 (1999).
10. H. Cherouat, M. Braci and S. Diop, "Vehicle Velocity, Side Slip Angles and Yaw Rate Estimation," *Proceedings of the IEEE International Symposium on Industrial Electronics*, Dubrovnik, Croatia, vol. 1 (2005) pp. 349–354.
11. Y. Aoki, T. Uchida and Y. Hori, "Experimental Demonstration of Body Slip Angle Control Based on a Novel Linear Observer for Electric Vehicle," *Industrial Electronics Society, IECON, 31st Annual Conference of IEEE*, Raleigh, North Carolina, USA (2005) pp. 2620–2625.
12. C. Ünsal and P. Kachroo, "Sliding mode measurement feedback control for antilock braking systems," *IEEE Trans. Control Syst. Technol.* **7**(2), 271–281 (1999).
13. J. Stéphant and A. Charara, "Virtual sensor: Application to vehicle sideslip angle and transversal forces," *IEEE Trans. Ind. Electron.* **51**(2), 278–289 (Apr. 2004).
14. J. C. Cadiou, A. E. Hadri and F. Chikhi, "Non-Linear Tyre Forces Estimation Based on Vehicle Dynamics Observation in a Finite Time," *Proc. Inst. Mech. Eng. [D]: J. Automob. Eng.* **218**, 1379–1392 (Jul. 2004).
15. Z. B. Song, Y. H. Zweiri, L. D. Seneviratne and K. Althoefer, "Non-linear observer for slip estimation of tracked vehicles," *Proc. Inst. Mech. Eng. [D]: J. Automob. Eng.* **222**(4), 515–533 (2008).
16. Z. B. Song, X. J. Song, K. Althoefer, Y. Zweiri and L. D. Seneviratne, "Non-Linear Observer for Slip Parameter Estimation of Unmanned Wheeled Vehicles," *IEEE International Conference on Mechatronics and Automation,* Harbin, Heilongjiang, China (2007).
17. P. F. Muir and C. P. Pneuma, "Kinematic modelling of wheeled vehicle," *Int. J. Rob. Res.* **4**(2), 281–329 (1987).
18. J. C. Alexander and J. H. Haddocks, "On the kinematics of wheeled mobile robots," *Int. J. Rob. Res.* **8**(5), 15–27 (1989).
19. H. S. Shim, J. H. Kim and K. Koch, "Variable Structure Control Nonholonomic Wheeled Mobile Robot," *Proceedings of the IEEE International Conference on Robotics and Automation,* Nagoya, Japan (1995) pp. 1694–1700.
20. R. M. Murray and S. S. Sastry, "Nonholonomic motion planning: Steering using sinusoids," *IEEE Trans. Automat. Control* **38**(5), 700–716 (1993).
21. K. Yoshida and G. Ishigami, "Steering Characteristics of a Rigid Wheel for Exploration on Loose Soil," *Proceedings of the IEEE/RSJ International Conference on Intelligent Robots and Systems,* Sendai, Japan (2006) pp. 3995–4000.
22. V. Utkin, J. Guldner and J. Shi, *Sliding Mode Control in Electromechanical Systems* (Taylor & Francis, Philadelphia, PA, 1999).
23. C. Edwards and S. K. Spurgeon, *Sliding Mode Control : Theory and Applications* (Taylor & Francis, London, 1998).
24. Y. H. Zweiri, J. F. Whidborne and L. D. Seneviratne, "Diesel Engine Indicated and Load Torque Estimation Using Sliding Mode Observer," *Proc. Inst. Mech. Eng. [D]: J. Automob. Eng.* **220**(6), 775–785 (2006).
25. A. T. Le, Modelling and Control of Tracked Vehicles, *Ph.D. Thesis* (Department of Mechanical Engineering, The University of Sydney, Jan. 1999).
26. Racelogic , Non-contact GPS speed and distance measurement, available at http://www.racelogic.co.uk/?show=VBOX (Last accessed on 15 Dec. 2007).
27. D. M. Helmick, Y. Cheng, D. S. Clouse and L. H. Matthies, "Path Following using Visual Odometry for a Mars Rover in High-Slip Environments," *IEEE Aerospace Conference Proceedings*, Big Sky, Montana (2004) pp. 772–789.
28. X. J. Song, L. D. Seneviratne, K. Althoefer, Z. B. Song and Y. Zweiri, "Visual Odometry for Velocity Estimation of UGVs," *IEEE International Conference on Mechatronics and Automation,* Harbin, Heilongjiang, China (2007).
29. M. S. Grewal and A. P. Andrews, *Kalman Filtering Theory and Practice Using Matlab* (John Wiley & Sons, Hoboken, New Jersey, 2001).

Appendices A. Extended Kalman Filter

This appendix presents the formulation of the EKF and the structure of the EKF is described.

The EKF is a recursive and minimum mean-square-error estimator.[29] It estimates the state of a dynamic system by combing observations from sensors with the state of prediction. This procedure is recursive; it means there is no need for reprocessing of previous observations to add a new set of observations. Noise is assumed to be a zero-mean, Gaussian distribution. A slip estimator is developed for the estimation of wheel slip and slip angle using the kinematic model.

Here, an extended kinematic model is used where wheel slip and slip angle are assumed to be slowly time-varying variables. This assumption is generally used in the design of the Kalman filter.[8] The state vector is $X = [X, Y, \theta, i, \alpha]^T$. The control input vector is $u_{k-1} = \delta_{k-1}$.

$$\dot{X} = V_x[\cos\phi - \tan\alpha \sin\phi] \tag{25}$$

$$\dot{Y} = V_x[\sin\phi + \tan\alpha \cos\phi] \tag{26}$$

$$\dot{\theta} = \frac{V_x}{r(1-i)} \tag{27}$$

$$\dot{i} = 0 \tag{28}$$

$$\dot{\alpha} = 0 \tag{29}$$

The following details the design of the EKF estimator for a single wheel moving over a terrain. The extended kinematic model can be converted into the following discrete-time representation using the first-order Euler method.

https://doi.org/10.1017/S0263574708005146 Published online by Cambridge University Press

The state variables are
$X_{k-1} = [X_{k-1},\ Y_{k-1},\ \theta_{k-1},\ i_{k-1},\ \alpha_{k-1}]^T$

$$X_k = f(X_{k-1}, u_{k-1}, v_{k-1}) =$$
$$\begin{bmatrix} X_{k-1} + \Delta T[\cos\phi_{k-1} - \tan\alpha_{k-1}\sin\phi_{k-1}]VX_{k-1} \\ Y_{k-1} + \Delta T[\sin\phi_{k-1} + \tan\alpha_{k-1}\cos\phi_{k-1}]VX_{k-1} \\ \theta_{k-1} + \Delta T\frac{VX_{k-1}}{r(1-i_{k-1})} \\ i_{k-1} \\ \alpha_{k-1} \end{bmatrix} \quad (30)$$

where $u_{k-1} = \delta_{k-1}$, VX is identical to V_x for simplification of symbols.

From Eqs. (5), (6) and (7), the kinematic equations are non-linear so that an EKF is required for the estimation. Process and observation models are as follows:

$$X_k = f\,[X_{k-1}, u_k] + v_k,$$
$$Z_k = h\,[X_k] + w_k,$$

where v_k is the process noise, z_k is the observation, w_k is the measurement noise and h is the function mapping the control inputs and the states to observation.

State estimate propagation is given by

$$\hat{X}_k(-) = F_{k-1}X_{k-1}(+),$$

where F is the state error transfer matrix, $F = \frac{\partial f_k}{\partial X}$, $F \in R^{5\times5}$

Error covariance estimate propagation is obtained as follows:

$$P_k(-) = F_{k-1}P_{k-1}(+)F_{k-1} + Q_{k-1},$$

where Q is spectral density matrix, initial value of matrix P is diag($[1e-4,\ 1e-4,\ 1e-4,\ 1e-4,\ 1e-4]$).

Kalman gain is computed as follows:

$$\bar{K}_k = P_k(-)H_k^T\left[H_kP_k(-)H_k^T + R_k\right]^{-1},$$

where R is noise covariance matrix, $R \in R^{3\times3}$. In this research, R is chosen as diag$[1e-6,\ 1e-6,\ 1e-6]$. Let $S = H_kP_k(-)H_k^T + R_k$ and $H = \frac{\partial h_k}{\partial X}$ and its value is [1 0 0 0 0; 0 1 0 0 0; 0 0 1 0 0].

State is updated as follows:

$$\hat{X}_k(+) = \hat{X}_k(-) + \bar{K}_k[z_k - H_k(\hat{X}_k(-))],$$

here, innov is used to represent the innovation error, innov = $z_k - H_k(\hat{X}_k(-))$.

Error covariance update is computed as follows:

$$P_k(+) = P_k(-) - \bar{K}_kH_kP_k(-).$$

B. Wheel Slip and Slip Angle Measurement Using the 2D Test Rig

Wheel slip and slip angle of a single wheel, i and α can be measured using the test rig in Figs. 4(a) and 4(b) as follows:

ω: measured by the wheel encoder [see Figs. 4(a) and 4(b)].

Outputs

α: measured using the arm rotary encoder, the arm linear encoder and the carriage encoder (see Figs. 5 and 6).

$$\alpha = \pi - (\theta_1 + \theta_2) + \delta_c$$

i: measured using the arm rotary encoder, the arm linear encoder, the carriage encoder and the wheel encoder [see Figs. 4(a) and 4(b)].

$$i = 1 - \frac{\sqrt{(\dot{r}\cos\theta_1 - r\sin\theta_1\dot{\theta}_1)^2 + (\dot{r}\sin\theta_1 + r\cos\theta_1\dot{\theta})^2}\cos\alpha}{\omega r}.$$

https://doi.org/10.1017/S0263574708005146 Published online by Cambridge University Press